CREATED USING THE RSC LaTeX PCCP ARTICLE TEMPLATE – SEE www.rsc.org/electronicfiles FOR DETAILS

Static friction scaling of physisorbed islands: the key is in the edge

Nicola Varini,[a,b] Andrea Vanossi,[c,d] Roberto Guerra,[d,c] Davide Mandelli,[d] Rosario Capozza,[d] and Erio Tosatti*[,d,c,e]

Received Xth XXXXXXXXXX 20XX, Accepted Xth XXXXXXXXX 20XX
First published on the web Xth XXXXXXXXXX 200X
DOI: 10.1039/b000000x

arXiv:1412.4993v1 [cond-mat.mes-hall] 16 Dec 2014

Abstract

The static friction preventing the free sliding of nanosized rare gas solid islands physisorbed on incommensurate crystalline surfaces is not completely understood. Simulations modeled on Kr/Pb(111) highlights the importance and the scaling behavior of the island's edge contribution to static friction.

1 Introduction

Static friction – sometimes desirable, often a nuisance, always important – is less studied than its more famous counterpart, dynamic friction. A standing puzzle is the persistence of static friction even for ideal mesoscale sized sliders such as incommensurate physisorbed islands on atomically perfect crystal surfaces, where one could expect it to asymptotically vanish. Here we show, based on prototype atomistic simulations of rare gas islands sliding on a crystal surface, that the slider's *edges* represent the ultimate actors. When the island body is ready to slide "superlubrically", the sliding is impeded by an edge-originated barrier that prevents the misfit dislocations or solitons – tiny density and corrugation modulations with the beat periodicity between adsorbate and surface – from moving. Only when the static friction force is reached, the barrier vanishes locally at one point on the edge, solitons enter through this point to sweep the island, which only then becomes depinned and free-sliding. We show that finite size scaling of static friction of a superlubric rare gas island with area A has the same form A^{γ_s} as discussed in literature for dynamic friction, but with specific, generally distinct static scaling exponents γ_s that are edge-controlled and smaller than 1/2, as opposed to $\gamma_s = 1$ for pinned, commensurate islands. The island static friction connection with edges, here addressed realistically in rare gas islands for the first time, constitutes the controlling factor for inertial depinning in quartz crystal microbalance experiments, and is expected to be a factor of importance for nanotribological applications involving weak contacts.

Understanding the atomic-scale mechanisms which control friction is probably one of the most important challenges in nanotechnology[1–4]. Static friction – the threshold force necessary to initiate the sliding between two contacting surfaces, which Coulomb distinguished historically from dynamic friction – is basic not just to our everyday experience, including standing and walking, but is crucial, and often fatal, to the working of nanosystems[5]. In nanomotive devices, as well as in elementary processes such as the pulling or pushing of nano-objects on a surface by a tip[6–8], or by a colliding molecule[9], or by simple inertia[11,12], static friction constitutes the ultimate obstacle that affects the onset of sliding. Often undesired, static friction of nano-sliders can also be of help, e.g., to prevent the diffusive sliding away of adsorbed molecules, small proteins clusters and of islands, favoring so-called nano-positioning when deposited on surfaces[13,14]. Despite its importance, and several notable exceptions[15–20], static friction is not as much discussed and qualified as dynamic friction, which is generally much more popular. Differently from macroscopic sliding where relatively complex processes due to asperities and multiple contacts[21], or to load inhomogeneity[15–17] are at play, homogeneous crystalline nano-sliders offer a unique oppor-

∗ tosatti@sissa.it
[a] *Research & Development, Curtin University, GPO Box U 1987, Perth 6845, Australia.*
[b] *iVEC, 26 Dick Perry Avenue, Kensington WA 6151, Australia.*
[c] *CNR-IOM Democritos National Simulation Center,Via Bonomea 265, I-34136 Trieste, Italy.*
[d] *International School for Advanced Studies (SISSA), Via Bonomea 265, I-34136 Trieste, Italy.*
[e] *International Centre for Theoretical Physics (ICTP), Strada Costiera 11 I-34151 Trieste, Italy.*

tunity to address static friction in its simplest form – that between perfectly regular, periodic faces.

Given two crystals in contact, e.g., a two-dimensional (2D) adsorbate monolayer island (the slider) and a perfect crystal surface (the substrate), different possibilities may occur. The island lattice may be commensurate (C) with the surface lattice, or it may be incommensurate (IC), meaning that the two lattice 2D cells cannot be made to coincide by any rational scale change p/q, where p and q are two integers. In the general C case, and also in the IC case if the slider is "soft" (inter-atomic forces weaker than or similar to the typical substrate corrugation forces, causing effective commensurability to prevail), the island will exhibit static friction, due to pinning of the two lattices. The latter situation of strong contact has been theoretically addressed by a number of workers[15–20,22,23]. Conversely, static friction should ideally vanish, foreshadowing free sliding, also called "superlubricity", for a prototype weak contact, such as an infinite, hard IC crystalline slider, weakly interacting with a perfectly periodic substrate[24–29].

Experimentally, very low friction dynamic sliding has been observed, e.g., in graphitic materials by extracting telescopic carbon nanotubes[31,32] or by rotating out of registry an AFM-tip driven graphite flake on a graphite substrate[33–35]. Evidence of low dynamic friction in non-crystalline sliding has been collected by AFM manipulation of amorphous and crystalline antimony nanoparticles deposited on a graphite substrate[6,7,36]. At the same time however the corresponding static friction, even if conceptually and practically different, and no less important, was generally skirted in these low-friction contacts. In recent studies of 2D incommensurate colloidal crystals sliding over optical lattices, static friction emerged clearly, along with a pinned-to-superlubric transition for decreasing periodic potential magnitudes[37–39]. Static friction controls directly the quartz crystal microbalance (QCM) sliding experiments[10–12] which we consider as our reference system. In QCM a crystal surface with a layer, but particularly a submonolayer coverage of physisorbed inert gas is periodically shaken to dislodge the 2D crystalline islands formed by coalescence of the adsorbed gas molecules, giving rise to inertial sliding friction. These submonolayer islands generally constitute incommensurate sliders[40], which as a rule should behave as hard (even if not at all rigid) since the gas interatomic energy, of order 15 meV, although much weaker than the atom-surface adhesive energy of order 150 meV, is usually much stronger than the substrate corrugation, typically only a few meV[41]. QCM data in UHV generally show that for low rare gas coverage, low temperature, and moderate oscillatory force magnitude, adsorbed islands remain stuck to the surface and do not slide, despite cleanliness, hardness and incommensurability[10,42–44]. The islands remain pinned by static friction until either the growing inertial force, or the increasing coverage – which implies a larger average island size[45] and thus a larger inertial force – or temperature, reach a threshold value. Only beyond that point, the static friction is overcome, the islands depin, and inertial sliding takes place, with a nonzero slip time whose inverse measures dynamic friction[10–12].

Our main goal is to understand the ultimate reason why static friction should persist even for ideally perfect rare gas islands adsorbed on crystalline surfaces, which constitute weak contacts where owing to incommensurability free superlubric sliding could be expected. Real-life surfaces are of course far from perfect, so that an adsorbed island will generally attach to surface steps, defects, impurities, etc., which can provide extrinsic pinning[18]. Nevertheless, static friction of cold adsorbed islands generally survives the progressive elimination of defects, and their pinning effect by reducing the oscillation amplitude[44,46,47]. For a defect free, genuinely incommensurate hard island, such as is realized for example by Kr/Pt(111)[48], and most other cases where the island-surface commensurability ratio is known to drift continuously with temperature, there should be no barrier and no pinning. Here an intrinsic source of static friction must be at work.

The edge is an intrinsic "defect" that every island, cluster, or deposited nanosystem, must have. We conducted simulations mimicking realistic 2D incommensurate rare gas islands up to very large size, adsorbed on defect free metal surfaces. These simulations clearly show that even without defects, these weak contacts exhibit a basic static friction threshold dictated by the island edges. Specifically, for an adsorbed island, where the misfit lattice-mismatched dislocations (i.e. solitons) pre-exist, we find that the entry through the island edge of a new soliton is the event that initiates the depinning and the subsequent superlubric sliding. Soliton entry however is not cost free; the pushing force must overcome an edge-related energy barrier, which is thus the controlling element of the island's static friction. The barrier's relative role and importance, and the ensuing static friction are found to decrease with increasing island size and temperature, precisely as seen in experiments. Since the static friction is edge-originated, its scaling $F_s \sim A^{\gamma_s}$ with the island's area A is not only sub-linear, $\gamma_s < 1$, but sub-linear even with respect to the coarse-grained island perimeter $2(A\pi)^{1/2}$, that is $\gamma_s < 1/2$, indicating that only a zero-measure subset of edge points is responsible for the pinning barrier. By contrast with this result for incommensurate islands we examine in parallel that of com-

This journal is © The Royal Society of Chemistry [year]

mensurate islands, strong contacts which have a "bulk" pinning, with a trivial area scaling exponent $\gamma_s = 1$. Even there nonetheless the edge plays a role. We find that the lattice dislocation triggering the sliding of a commensurate island nucleates, as also discussed by previous workers in different situations [15–17], preferentially at the island edge, here acting therefore as a facilitating element which quantitatively reduces the static friction.

In the far more common case (for physisorption) of incommensurate islands, we will identify, at the general level, the emerging key parameters which control edge-induced static friction. They are: a) the shape, rugosity, and elasticity of the island edge, which influence γ_s, a sublinear size scaling exponent that does not appear to exhibit universality; b) the amplitude of the substrate corrugation potential, which controls the static friction magnitude; c) the temperature, influencing static friction both directly, and indirectly through the island's changing incommensurability.

The role of edge-induced static friction is, we propose, especially important for QCM experiments, a context in which it has apparently not been previously discussed. As was said above, it is a general observation in QCM that lack of inertial sliding, and a consequent zero slip time, occurs in all cases for a sufficiently low coverage and low temperature, a regime where the adsorbate forms crystalline islands that are generally incommensurate with a crystalline substrate [10–12,40,44,46,47]. We will show that realistic parameters for the adsorbed rare gas on a metal surface predict that the QCM inertial force cannot reach, as coverage increases, the low temperature static friction threshold for depinning until the island diameters grow as large as many tens when not a hundred of nanometers. That is a remarkably large size, comparable to that of terraces or facets of even a good quality metal surface. The conclusion is thus that intrinsic edge pinning is not just qualitatively, but quantitatively important in QCM and other incommensurate nano-sliding experiments. We also find that the effects of temperature are diverse and intriguing. Besides increasing the edge rugosity, temperature does reduce the effective substrate corrugation, which in turn lowers the static friction threshold. At the same time, the commensurability ratio of the two lattices may drift with temperature because the island's thermal expansion is generally unmatched by that of a metal substrate. As temperature grows, one or more low order commensurabilities may accidentally be hit, at which point a geometrical interlocking barrier against sliding arises, leading in principle to the novel possibility of reentrant static friction.

2 MD simulations of rare gas islands and their static friction on a metal surface: Kr/Pb(111)

To substantiate our discussion with a specific case study, we model an incommensurate rare gas island on a metal surface with parameters appropriate to Kr/Pb(111), a prototype system of current interest [47] which we adopt here as a generic model hard slider. The atoms interact mutually via Lennard-Jones forces (standard parameters given in Methods). We restrict to temperatures well below half the adsorbate bulk melting temperature, $T \ll T_m/2$ (for $T_m = 115\,\mathrm{K}$, we employ $T \ll 60\,\mathrm{K}$), where the adsorbate island does not yet melt, remaining crystalline with a 2D triangular lattice only weakly modulated by the incommensurate and essentially rigid underlying (111) metal substrate. For different assumed shapes we simulate a sequence of islands consisting of N adsorbate atoms, with N increasing up to a maximum size of about 300000. Using molecular dynamics we first relax and anneal the islands – initially cut out of a perfect triangular lattice – in the (111) periodic potential mimicking the perfect crystal substrate, and optimize the overall island adsorption geometry so as to minimize energy. In the resulting zero temperature state, the main interior part of the island and the substrate are incommensurate, with the model Kr atom-atom spacing $a = 4.057\,\text{Å}$ only slightly smaller than $(7/6)a_s = 4.084\,\text{Å}$, where $a_s = 3.50$ Å is the nearest neighbor distance in Pb(111).

The surface-deposited islands develop delicately regular soliton superstructures, representing the deviation from exact (6/7) commensurability, as pictured in blue scale in Fig. 1 by means of a contrast enhancement technique (see Methods). These pictures highlight the great deformability of this gossamer superstructure, well beyond any rigid or nearly rigid approximation. Compressional/dilational strains in the 2D lattice are directly reflected by increased/decreased density of superstructures.

3 Island depinning and size scaling of static friction

We subsequently simulate the forced depinning of the island (previously prepared at a desired temperature using a thermostat, then switched off, see Methods), by applying to the island center of mass a constant planar total force F_{ext}, that is by applying to each Kr atom a force F_{ext}/N. In our protocol the static friction is the lowest value of F_{ext} sufficient to cause, within 1.2 ns simulation time, a center-of-mass drift of two substrate interatomic spacings, or 0.7 nm, signaling the depinning of the is-

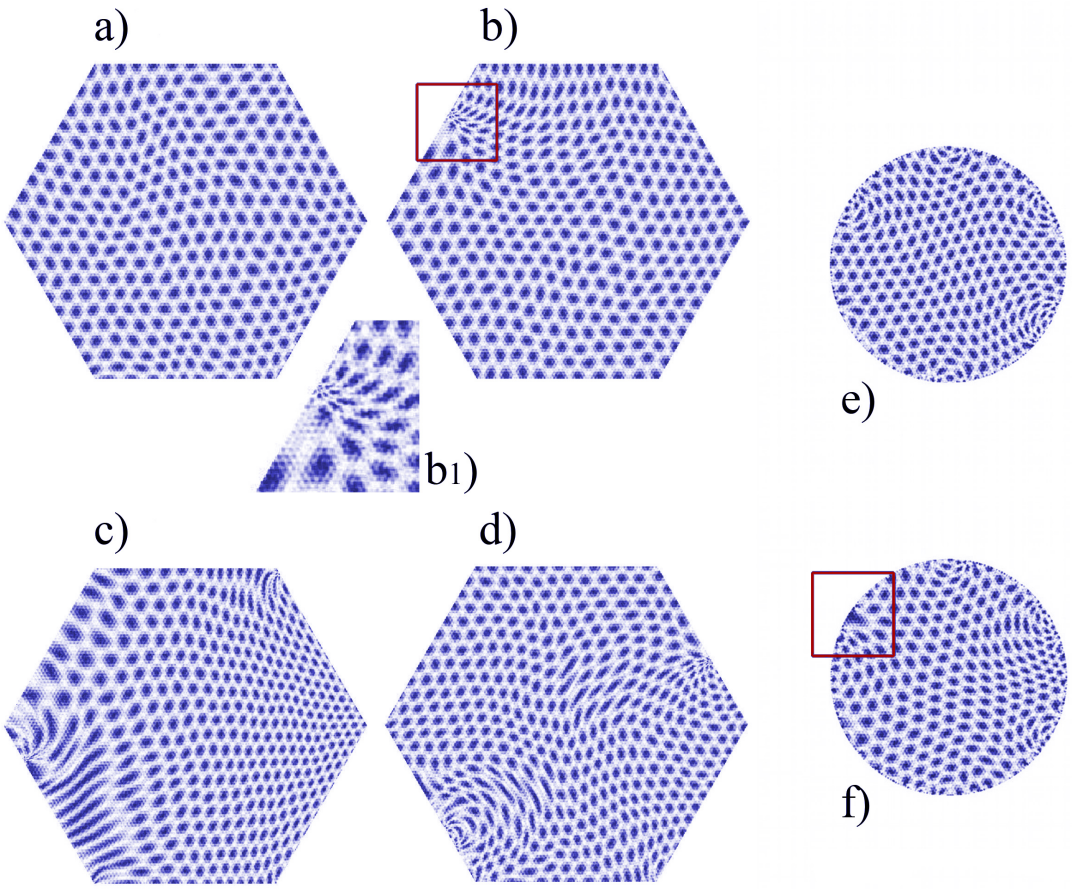

Fig. 1 Model ideal hexagonal ($N = 269101$) and circular ($N = 177507$) Kr islands adsorbed on Pb(111). Pictures show maps of the island, with colors ranging from dark blue when Kr atoms are maximally coincident with a (6/7) rescaling of the underlying Pb atom positions, to clear when they are minimally coincident. The resulting Moiré patterns, enhanced in this manner for visibility (see Methods) highlight the soliton network between the island and surface lattices and their evolution at the static friction threshold. (a) After annealing, at zero temperature and zero applied force ($T = 0$, $F_{ext} = 0$); (b) with applied force $F_{ext} = 1.4\,\mathrm{eV/\AA}$, just above the static friction value, and right after the soliton entry at a left edge corner – highlighted by the red square and magnified by the zoomed in region (b1); (c) same system after sliding of the island center by one surface lattice spacing. Note the density accumulation at the front edge and rarefaction at the trailing edge, showing the frictional role of the edges; (d) same system at later time when the sliding is 1.5 lattice spacings, and a soliton exits the island on the right hand side. (e) Circular island, just after annealing ($T = 0$, $F_{ext} = 0$); (f) with applied F_{ext} slightly above the static friction threshold. Here again the static friction is determined by the entry of a soliton at the left edge, highlighted by the red square.

This journal is © The Royal Society of Chemistry [year]

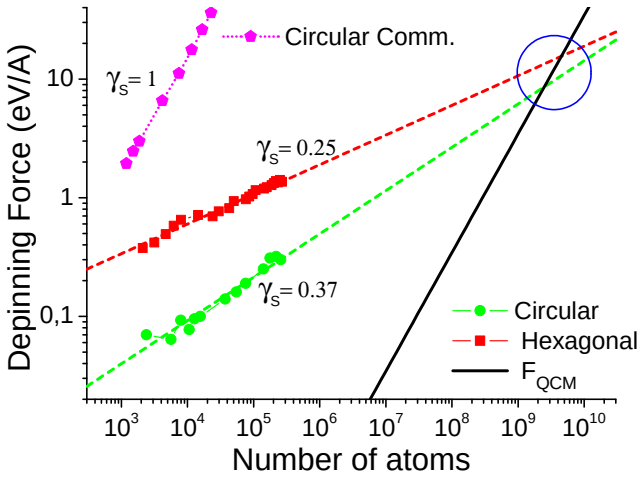

Fig. 2 Size scaling of total static friction force F_s of simulated incommensurate adsorbed islands (modeled on Kr/Pb(111)) at $T = 0\,\mathrm{K}$ as a function of the atom number N (log-log scale) for *i*) hexagonal islands (squares); *ii)* circular islands (circles). Assumed surface corrugation: 5% of the atom adsorption energy; note the strongly sublinear scaling for both shapes. The intersection with the estimated QCM inertial force (black solid line) is emphasized (blue circle), showing how the edge-originated static friction alone can prevent island sliding up to large island sizes, which qualitatively corresponds to large sub-monolayer adsorbate coverages. By comparison we also show the size scaling of static friction ($\gamma_s = 1$) for a *commensurate* adsorbate at $T = 50\,\mathrm{K}$ (see Methods). The commensurate frictional stress F_s/A is about $10^7 N/m^2$ compared with a much smaller 40 N/m^2 of incommensurate islands at inertial depinning.

land[49]. The shapes of the island edge, in principle quite important for static friction, are not easily equilibrated in MD simulations at the low temperatures considered. We therefore examine two ideally opposite test shapes, perfect hexagonal and circular – neither of them realistic but providing together a fair idea of the generic behaviour to be expected. Torques and sliding-induced overall rotations arising from possible non-centered island shapes are also neglected. Despite the natural random asymmetry expected of realistic islands, their large size prevents the brownian motion of their orientations (as well as of their centers of mass) making the torque needed to cause their overall rotation generally very large for QCM.

Fig. 2 shows, in log-log scale, the overall static friction force $F_0(N)$ necessary to depin the hexagonal and the circular incommensurate islands made up of N atoms. In alternative to that, to represent a commensurate case we also simulate the depinning of a model now representing $\sqrt{3}\times\sqrt{3}$ islands, obtained with potentials of similar amplitudes but no longer incommensurate and no longer at very low temperature (where kinetics would be too slow) but at a reasonably high temperature near 50 K (details in Methods).

Our main result is that the static friction of incommensurate islands is very small but nonzero, and interestingly area-dependent. For each given shape the static friction obeys with striking precision a power law scaling $F_s \sim F_0(A/\Sigma)^{\gamma_s}$ where $\Sigma = a^2\sqrt{3}/2$ is the area per adsorbed atom. The incommensurate exponent γ_s varies between 0.25 and 0.37 depending on the choice of edge morphology, here polygonal or circular, respectively. While of course real islands will generally look like neither, the two cases provide reasonably extreme instances, the circular probably more realistic than the polygonal, in virtue of its greater variety of edge atom configurations. We further show that in both shapes the island static friction barrier resides in a small set of points on the edge, as a consequence of which the static friction exponent γ_s is definitely less than 1/2, the value expected if the density of the pinning points on the edge was uniform.

The commensurate island static friction obtained in simulation is by comparison five to six orders of magnitude larger than the incommensurate static friction, which demonstrates and emphasizes the huge gap between a strong and a weak contact. With increasing island size, we find that the commensurate friction force F_s grows proportionally to the area, $\gamma_s = 1$, as expected when the bulk of the island participates in the static friction barrier, resulting in a static friction stress F_s/A independent of area.

The size-independent static friction shear stress F_s/A for our model commensurate islands of small size is about $10^7 N/m^2$. We can compare that with the nominal theoretical interface stress of a rare gas on metal (G/M) interface $\mu_{G/M} = \frac{2\mu_G\mu_M}{\mu_G+\mu_M} \simeq 1.16 * 10^9 N/m^2$ (where $\mu \equiv C_{44}$ are the respective bulk shear elastic constants, here of Kr and Pb), to conclude that the commensurate island static friction stress obtained is about $10^{-2}\mu_{G/M}$. Interestingly, that falls inside the range $\mu_{G/M}/30 \div \mu_{G/M}/1300$ expected from dislocation theory of macroscopic, commensurate and inhomogeneous strong contacts.[15–17].

Returning to our main system of interest, the simulated incommensurate Kr/Pb islands, the shear stress F_s/A is many orders of magnitude smaller than the commensurate, and unlike that case is clearly size-dependent. A physically relevant island area where we wish to evaluate the static friction force $F_s(A)$ is the critical area at which it equals the peak inertial force in a QCM experiment, $F_{QCM}(A_{crit}) = \rho A_{crit}\Delta(2\pi f)^2$, where ρ is the adsorbate 2D mass density, Δ the QCM oscillation amplitude, f the frequency. Only in islands whose area exceeds A_{crit}

the inertial force exceeds static friction, and inertial depinning followed by dynamic frictional sliding can take place. Experimental QCM orders of magnitude being $\Delta \sim 100\,\text{Å}$, $f \sim 10$ MHz yield an inertial force which grows linearly with A and crosses, as shown in Fig. 2, the static friction lines $F_s/A_{crit} = F_{QCM}/A_{crit}$, signaling depinning above a critical area

$$A_{crit}/\Sigma \sim \left(\frac{F_0}{\Sigma\rho\Delta(2\pi f)^2}\right)^{\frac{1}{1-\gamma}}. \qquad (1)$$

The incommensurate island data of Fig. 2, obtained for an assumed 5% Pb(111) substrate corrugation, yields $N_{crit} = A_{crit}/\Sigma \simeq 3 \cdot 10^9$, or $A_{crit} \simeq 4.3 \cdot 10^{10}$ Å^2.

That amounts to island diameters of the order of several microns, corresponding to an inertial static friction force of order 16 nN, equivalent to a QCM depinning stress $\simeq 40N/m^2$, more than seven orders of magnitude smaller than $\mu_{Kr/Pb}$, and more than five orders of magnitude smaller than the commensurate island static friction stress $\simeq 10^7 N/m^2$. Qualitatively similar data are found for lower corrugations, where the static friction force and thus the critical depinning area A_{crit} drops by a factor $\sim 5 \div 15$ when the corrugation is decreased from a large 5% (where phenomena are easier to study) to $2 \div 1\%$.

At larger incommensurate lattice mismatch, and under the effect of temperature the critical island size for depinning and the static friction shear stress will be correspondingly smaller, but we still expect large critical island diameters ranging from many tens to hundreds of nanometers.

Incommensurate islands smaller than this size will remain pinned by their own edge, and only larger ones will overcome the edge-originated static friction and slide inertially in QCM. These large estimated critical radii constitute a strong result of this work: the intrinsic edge-related static friction is by no means a small or academic effect, as one might initially have expected. Strong as it is, the edge contribution can in fact add significantly to impurity and defect pinning [19], even after renormalization of F_s caused by edge roughness and temperature. The order of magnitude obtained for the critical depinning island size must be compared with the general experimental observation of a critical adsorbate coverage of 5-30% below which static friction wins, there is no low temperature inertial depinning, and the slip time remains zero even on the cleanest surface, and even for small oscillation amplitudes, a regime where dilute defects play a smaller role. If a real surface is crudely assumed to consist of terraces of hundreds nanometers in size, the A_{crit} corresponds to a non negligible submonolayer coverage, in agreement with experimental observations, such as e.g., in Ne on Pb(111) [44,47]. For a strongly commensurate island conversely the inertial force $F_{QCM}(A)$ and the static friction force F_s are both proportional to A and do not cross as A grows, indicating that the island will not inertially depin and remain stuck by its own bulk static friction, at least until larger island sizes and temperatures outside of this study.

4 Edge pinning and soliton flow

We can now address the question, what is the physics of edge-induced pinning? One key observation is that in order for an island with lattice parameter a to slide over the surface with lattice spacing b, the misfit soliton lattice, of spacing $[\frac{a}{b} - 1]^{-1}$, must *flow* across the island in the sliding direction with a much larger speed $v[\frac{a}{b} - 1]^{-1}$ than the overall island speed v – solitons must move very fast in order for the island to move even slowly (see Supplementary Movie 1). The sublinear size scaling of F_s with $\gamma_s < 1/2$ in Fig. 2 occurs because solitons enter the island through specific points and not everywhere along the edge – a corner in the perfect hexagonal shape for example as seen in the movie – and then sweep past, setting the island's soliton pattern in a state of flow. The motion of solitons is necessary for the island to slide. By preventing the free motion of solitons, which implies their free entry and exit, the island edges cause static friction. The local planar density of atoms for an edge-pinned island at pulling force just below the static friction threshold shows an accumulation on the island front and a rarefaction on the back side (see Supplementary Figure 1), also demonstrating the importance of non-rigid effects in larger regions surrounding the edge – the pinning agent. The edge adatoms lower their potential energy by settling in local minima, thus breaking the ideal island-surface translational invariance. We note incidentally that the settling of edge atoms also implies a local vertical deformation, besides a horizontal one, of the island boundary [35]. The overall relaxation gives rise to an edge related ("Peierls-Nabarro") energy barrier for the motion of solitons into and out of the island: the 2D edges cause the nominally incommensurate island to become stuck and pinned against sliding.

The observed depinning phenomenology with solitons getting in and out of the island edge resembles that of the caterpillar-like motion of the finite one-dimensional (1D) Frenkel-Kontorova (FK) model, where an edge barrier opposing kink motion gives rise to static friction [28]. Many additional 2D factors, such as sliding-induced relative lattice orientation, island shape, vertical relaxations, edge rugosity, adsorbate elasticity, etc., will enter in determining the exact value of the sublinear γ_s exponent, whose

This journal is © The Royal Society of Chemistry [year]

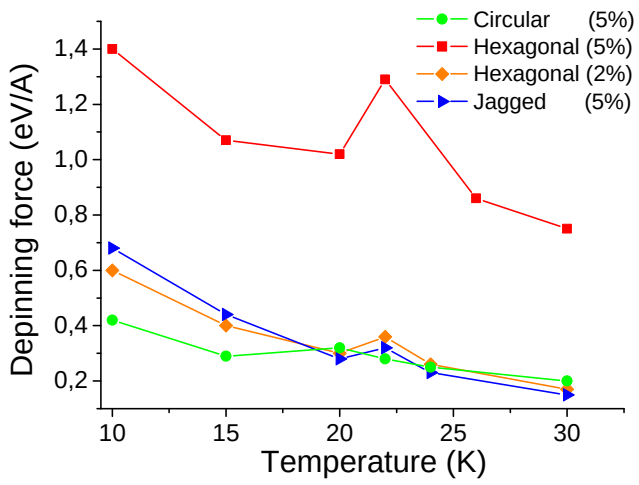

Fig. 3 Static friction force F_s as a function of temperature, for differently shaped islands (hexagonal, circular, and jagged, of about $3{\cdot}10^5$ atoms) and substrate energy corrugations (between 2 and 5 % of the atom adsorption energy). Superposed to the general decrease, the visible peak at 22 K reflects the low order adsorbate-surface 6/7 commensurability accidentally hit due to the island thermal expansion. This kind of accident, here portrayed for our model of Kr/Pb(111), might more generally lead to re-entrant pinning in QCM.

nontrivial theoretical description we do not attempt here.

5 Temperature effects

We come finally to discuss the effects of temperature on the edge-dependent static friction of incommensurate islands. The thermal evolution of static friction provided by simulations is shown in Fig. 3 for the hexagonal, circular, and jagged islands (See Methods), and for different substrate energy corrugations. Not surprisingly, thermal fluctuations facilitate the reduction of edge energy barriers, lowering static friction and favoring island depinning under the action of F_{ext}.

A second temperature effect will be to enhance thermal roughening of the island's edge, via adatom migration and 2D evaporation-condensation processes. The edge irregularity slightly modifies the overall soliton map in the island, especially close to the edge atoms that are stuck, a factor probably impacting the tribological response of the system, although most likely not more than shown by the difference between hexagonal and circular islands.

A third temperature effect is the anharmonic thermal expansion of the island's 2D lattice against the metal substrate, not yet expanding at these low temperatures. This thermal drift of lattice parameter ratio between the two crystalline surfaces in contact results in an alteration of the interface commensurability with consequences on static friction. In the chosen example of Kr/Pb(111), the relative registry is expected to drift from frank incommensurability at 10 K to a "6/7" higher order commensurability near 20-25 K and then again to incommensurability above that temperature. In our simulations this accidental, weak high-order commensurability gives rise to a temporary rise of static friction (Fig. 3). Even if the effect is not strong, and is sensitively dependent upon unknowns such as the edge rugosity and the substrate crystalline corrugation magnitude, in our realization we observe a small but visible peak of the temperature-dependent static friction for all the simulated island shapes. As highlighted in Fig. 4, the corresponding smearing in the pattern of the soliton network, the hallmark of an enhanced interface commensurability, for $T = 22$ K (hexagonal island) and $T = 20$ K (circular island) is visible and pronounced. This is suggestive of a more general possibility of expansion-induced reentrant static friction peaking around a commensurate phase.

We note as an aside that since incommensurability relative to 6/7 switches from overdense below 22 K to underdense above, the solitons are replaced in the process by antisolitons, entities which unlike solitons flow in the opposite direction to the applied force. The antisolitons being essentially lines of vacancies in the 2D lattice, their properties differ quantitatively from those of solitons, which are lines of interstitials. Antisolitons are generally of narrower width and less mobile, as seen for example in simulated sliding colloid monolayers[38], another system where some of the present results could in the future be verified – although the nature and pinning role of boundaries may be quantitatively different in that case. Although the resulting quantitative asymmetry between underdense islands (with stronger static friction) and overdense ones (with weaker static friction) should not directly affect the critical exponents, it might do so indirectly by affecting differently the island edge shape and rugosity. The above was for incommensurate islands. Very large at low temperatures the static friction of a commensurate island (see Methods) is crucially temperature dependent. It requires the thermal nucleation of a forward displaced domain. The activation time t_a for nucleation is expected to behave as in the edge-free bulk case[22,23]

$$t_a \sim C \exp(E_b/k_B T) \qquad (2)$$

where E_b is the effective activation energy barrier, lowered by the applied external force, and dependent on the nucleation site. As shown in Supplementary Movie 2, the island slides upon the temperature-related appearance of the nucleus at the island edge, followed by a subsequent

force-driven expansion. Here once again the edge plays an important role, even if different, in commensurate island static friction. Nucleation at the edge implies that (owing to greater atom mobility) there is a lower edge value E_b^e of the barrier relative to the bulk barrier E_b which controls homogeneous nucleation[22]. Since t_a establishes the threshold of depinning (see Methods), one obtains for commensurate islands of increasing size a constant t_a, i.e. a constant E_b, only if the applied force grows linearly with N, and therefore is $F_s \propto A$, or $\gamma_s = 1$, exactly like in homogeneous nucleation. We note incidentally that the same bulk-like static fricton scaling exponent $\gamma_s = 1$ should also occur for "soft" incommensurate islands, whose free sliding is dynamically unaccessible[24]. By contrast, for hard incommensurate islands the external force is resisted only by the edge pinning barrier, and therefore F_s will grow at most as $\sqrt{A}$ for a constant E_b^e. In real incommensurate islands the inhomogeneous stress along the edge further reduces E_b at specific points, causing the above-discussed sublinear size scaling of F_s with $\gamma_s < 1/2$.

6 Discussion and conclusions

We have conducted, in summary, a simulation study of atomistic sliding exhibiting static friction, an important tribological parameter whose physics had been, despite specific case studies[15–20,22,23,50], still insufficiently addressed so far for weak incommensurate contacts. With an eye to adsorbed rare gases typical of QCM experiments we simulated the forced depinning of islands, and found that the island edges play an all-important role, blocking especially the onset of otherwise superlubric sliding below a critical diameter. For rare gas islands inertially pushed on metal substrates, the edge-originated static friction is relevant, hindering the low temperature sliding of islands whose interior would otherwise be superlubric. Static friction is predicted for these islands to obey a sublinear scaling growth with island area, with an exponent roughly between 0.25 and 0.37, depending on the island shape. Previous work by Sorensen et al.[50] showed some effects due to edges of an AFM-like sliding of a Cu tip on a Cu surface. More recently, the *dynamic* sliding friction, in principle a different quantity from static friction, was studied in nanomanipulation experiments by Schirmeisen's group and found to obey a sublinear scaling laws[7].

That raises the conceptually interesting question of what should be the mutual relationship evolution of static and dynamic friction when size grows. This question is presently open, since it is hard to extract reliable dynamic friction size scaling from simulation, whereas conversely

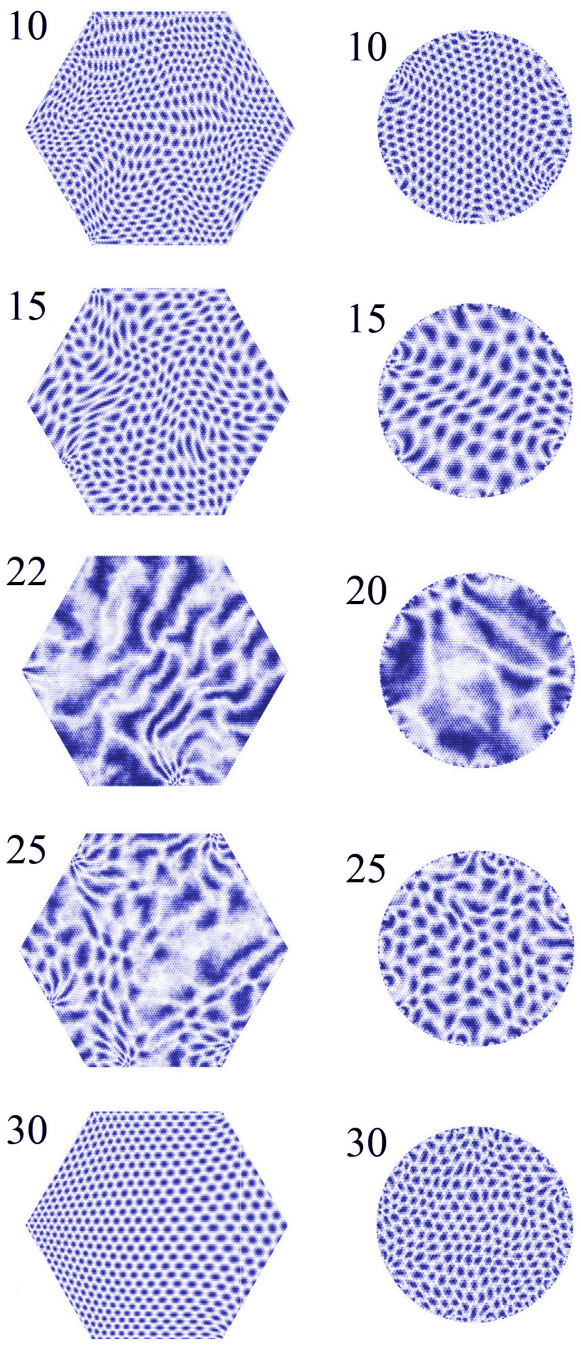

Fig. 4 Thermal evolution of the soliton network portrayed for hexagonal and circular shaped islands using the contrast enhancement technique for the lateral density variations relative to a 6/7 commensurability (see Methods). The island thermally expands, going from relatively overdense at low temperatures to underdense at high temperatures, thus exhibiting accidental near commensurability around 20-22 K.

This journal is © The Royal Society of Chemistry [year]

the experiments cannot directly address the static friction and its scaling laws. The lack of distinction found in some literature between static and dynamic friction remains in need of justification. The dynamic friction force $\mathcal{F}$ of a hard incommensurate island will consist of $\mathcal{F}_b+\mathcal{F}_e$, namely a bulk term plus an edge term. The edge term $\mathcal{F}_e$ should size-scale sublinearly like static friction with an exponent smaller than 1/2, and will in case of stick-slip also imply a sublinear dependence upon center-of-mass sliding speed. The bulk term $\mathcal{F}_b$ (vanishing in the static case) should conversely reflect superlubricity, with a linear, viscous speed dependence, and a bulk-like size scaling exponent $\gamma = 1$. For large speed and large island size the bulk dynamic friction will eventually prevail, with a size dependence very different from that of static friction. At much lower speed and at moderate size the bulk contribution should become less important, until eventually both static and dynamic friction should become edge-dominated, with a similar sublinear size scaling.

It will be very interesting to watch a future expansion of experimental data to verify if static friction will or not follow scaling laws we find here, with possible modifications when islands are replaced by metal clusters with considerably more rigid edges and stronger contacts, or in the case of 2D colloids, where edges may be completely different. The possible future use of QCM substrates with controlled size terraces, obtained e.g. by vicinal surfaces, should enable a verification of the static friction phenomena described here. The dependence of the static friction upon temperature is another result that could be experimentally pursued, while an estimate of the substrate corrugation magnitude, a generally unknown parameter, could be obtained by comparing data and simulations. More generally, the role of the edges of incommensurate sliding islands and clusters, not sufficiently emphasized until recently, must be acknowledged as an important source of static friction.

7 Computational Details

7.1 Model interactions

In our model the Pb(111) hard substrate is treated as a fixed and rigid triangular lattice frame, exerting on the mobile Kr adatoms an average attractive potential $V \sim$-150 meV, and a weak corrugation $\Delta V/V$ roughly in the range 2-5% between the on-top Pb site (the energy is minimum for a Kr adatom), and the hollow Pb site (energy maximum). Each Kr adatom is thus submitted to the overall potential $V = V_{\mathrm{Kr-Kr}} + V_{\mathrm{Kr-Pb}}$. The Kr-Kr interaction is modeled as regular Lennard-Jones (LJ) potential, with $\epsilon = 0.014\,\mathrm{eV}$ and $\sigma = 3.65\,\text{Å}$. Tiny corrections due to three-body forces as well as substrate-induced modifications of this two-body force are ignored. The Kr-Pb interaction is modeled by the following Morse-modified potential:

$$V_{\mathrm{Kr-Pb}} = \alpha(x,y)\left(\mathrm{e}^{-2\beta(\mathrm{z}-\mathrm{z}_0)} - 2\mathrm{e}^{\beta(\mathrm{z}-\mathrm{z}_0)}\right). \qquad (3)$$

The (111) structure of the substrate is accounted for by replacing the function $\alpha(x,y)$, that must exhibit the same periodicity of the underlying triangular lattice (we neglect here the small differences between fcc and hcp stacking sites). To represent the substrate modulation, we make use of the function

$$M(x,y) = \frac{2}{3} - \frac{4}{9}\cos\left(\frac{2\pi x}{b}\right)\cos\left(\frac{2\pi y}{\sqrt{3}b}\right) - \frac{2}{9}\cos\left(\frac{4\pi y}{\sqrt{3}b}\right). \qquad (4)$$

The constant b is the nearest neighbor distance of surface atoms. The modulating function $M(x,y)$ has been normalized to span the interval from 0 (top sites) to 1 (hollow sites). Back now to the Morse potential, the energy parameter is given by $\alpha(x,y) = \alpha^{top} + M(x,y)(\alpha^{hollow} - \alpha^{top})$ (see Supplementary for parameter details).

The LJ parameters leads to a nearest neighbor Kr-Kr distance which at 10 K (the lowest temperature of validity of our classical simulations, roughly equal to the temperature of quantum freezing in Kr) is close to the 3D experimental value of 4.01 Å, in turn 13% higher than the Pb-Pb triangular substrate nearest neighbor distance of 3.50 Å. Thus, the island and substrate 2D lattices are incommensurate with a ratio of 0.8728 at $T = 10\,\mathrm{K}$. Upon moderate heating, the island readily expands but the substrate does not. The closest strong commensuration of $6/7 = 0.8571$ of Kr/Pb(111) is reached and surpassed near $T \approx 20 - 22\,\mathrm{K}$.

To model the commensurate islands we reparametrized the substrate potential in order to match adhesion and corrugation energies of 190 meV and 1.9 meV, respectively, and a lattice constant of $3.61/\sqrt{2}$ Å, borrowing them from the Xe/Cu(111) case[22]. Starting from a Xe-Xe Lennard-Jones energy $\epsilon = 20\,\mathrm{meV}$, we used an ad-hoc $\sigma = 3.90\,\text{Å}$ in order to fictitiously match, at $\mathrm{T} = 50\,\mathrm{K}$, the $\sqrt{3}\times\sqrt{3}$ Cu(111) spacing.

7.2 Simulation procedure

To simulate QCM depinning, we applied to all atoms of the annealed adsorbate island (see below) a constant planar force. (This is adequate because the QCM oscillation period of $\sim 10^{-7}\,s$ is much longer than our simulation times). Static friction was measured in incommensurate systems using the following protocol: (i) an initial 1.2 ns annealing run at $T = 25\,\mathrm{K}$, with no force

applied ($F_{ext} = 0$); (ii) a 1.2 ns run at $T = 0\,\mathrm{K}$, with typical Berendsen thermostat constant $\tau = 100$ ps and still $F = 0$; (iii) the thermostat is removed, and a series of 1.2 ns runs at 0 K, with F applied instantaneously after the annealing procedure.

Simulations of commensurate systems were performed at $T = 50\,\mathrm{K}$. Similarly to above, we increased the external force from zero to F_s, at increments of $0.01\,\mathrm{meV/atom}$, letting the simulation evolve for 100 ps after each force step. In all cases, a displacement of the island center-of-mass by 2 lattice spacing within the same force step is taken as the signal of depinning. The static friction so obtained should depend slightly on the waiting time, but we verified that the decrease due to thermal barrier hopping was negligible with a waiting time longer than 1.2 ns.

At sufficiently low temperature and small size, the adsorbate atoms form spontaneously a triangular lattice weakly distorted by the underlying substrate. With the realistic choice $\sigma = 3.65\,\text{Å}$ for the LJ potential of krypton, the ideal 2D lattice has a spacing $a = 4.0568\,\text{Å}$. Exact 6/7 commensurability would require the slightly larger value 4.0842 Å. Due to this mismatch, the adsorbate island shows commensurate domains joined by bands of higher atomic density: the solitons, whose exact pattern depends on parameters, such as the temperature and the island size. To visualize the soliton superstructures, we developed a method exploiting information from all the adsorbed atoms. If the krypton atoms would occupy the position of a perfect triangular lattice with commensurability ratio 6/7, a uniform dilation by a factor 6 would map each adatom onto a position on top of a substrate atom.Thus, given an atom with coordinates (x, y, z), its dilated position $(X, Y, Z) = (6x, 6y, 6z)$ must render the modulating function M (Eq. 4) equal to zero, in the commensurate domains. The solitons, characterized by an enhanced mobility due to the mismatch with the substrate, are instead regions with $M(6x, 6y) \gtrsim 0$. Plotting each atom in bluescale, ranging from blue to white according to increasing values of $M(6x, 6y)$, the commensurate domains appear dark blue and the solitons as white bands.

8 Acknowledgements

We especially acknowledge early collaboration with U. Tartaglino and F. Ercolessi, and helpful discussions with N. Manini. The work was partly funded by the Swiss National Science Foundation through a SINERGIA contract CRSII2_136287, by PRIN/COFIN Contract 2010LLKJBX 004, by COST Action MP1303, and mainly by the ERC Advanced Grant No. 320796-MODPHYSFRICT. The CINECA supercomputing center is also gratefully acknowledged.

References

1 B. Bhushan, J.N. Israelachvili and U. Landman, *Nature*, 2002, **374**, 607.
2 M. Urbakh, J. Klafter, D. Gourdon and J.N. Israelachvili, *Nature*, 2004, **430**, 525.
3 M. Urbakh and E. Meyer, *Nature Mater.*, 2010, **9**, 8.
4 A. Vanossi, N. Manini, M. Urbakh, S. Zapperi and E. Tosatti, *Rev. Mod. Phys.*, 2013, **85**, 529.
5 J.W.M. Frenken, *Nature Nanotech.*, 2006, **1**, 20.
6 D. Dietzel, C. Ritter, T. Mönninghoff, H. Fuchs, A. Schirmeisen and U.D. Schwarz, *Phys. Rev. Lett.*, 2008, **101**, 125505.
7 D. Dietzel, M. Feldmann, U.D. Schwarz, H. Fuchs and A. Schirmeisen, *Phys. Rev. Lett.*, 2013, **111**, 235502.
8 S. Kawai et al., *Proc. Natl. Acad. Sci. USA*, 2014, **111**, 3968.
9 H. Hedgeland, P. Fouquet, A.P. Jardine, G. Alexandrowicz, W. Allison and J. Ellis, *Nature Phys.* 2009, **5**, 561.
10 A.Carlin, L. Bruschi, M. Ferrari, G. Mistura, *Phys. Rev.*, 2003, **68**, 045420.
11 J. Krim, *Nano Today*, 2007, **2**, 38.
12 J. Krim, *Adv. Phys.*, 2012, **61**, 155.
13 T. Junno, K. Deppert, L. Montelius and L. Samuelson, *Appl. Phys. Lett.*, 1995, **66**, 3627.
14 M. Sitti and H. Hashimoto, *IEEE-ASME Trans. Mechatron.*, 2000, **5**, 199.
15 J. A. Hurtado and K.-S. Kim, *Proc. R. Soc. Lond. A*, 1999, **455**, 3363.
16 J. A. Hurtado and K.-S. Kim, *Proc. R. Soc. Lond. A*, 1999, **455**, 3385.
17 Y. Gao, *J. Mech. Phys. Solids*, 2010, **58**, 2023.
18 G. He, M.H. Muser and M.O. Robbins, *Science*, 1999, **284**, 1650.
19 M.H. Müser, L. Wenning and M. O. Robbins, *Phys. Rev. Lett.*, 2001, **86**, 1295.
20 M.H. Müser, M. Urbakh and M.O. Robbins, *Adv. Chem. Phys.*, 2003, **126**, 187.
21 B.N.J. Persson, *Sliding Friction: Physical Principles and Applications*, Springer, 1998.
22 M. Reguzzoni, M. Ferrario, S. Zapperi and C. Righi, *Proc. Natl. Acad. Sci. USA*, 2010, **107**, 1311.
23 J. Hasnain, S.Jungblut and C. Dellago, *Soft Matter*, 2013, **9**, 5867.
24 M. Peyrard and S. Aubry, *J. Phys. Condens. Matter*, 1983, **16**, 1593.
25 M. Hirano and K. Shinjo, *Phys. Rev. B*, 1990, **41**, 11387.
26 K. Shinjo and M. Hirano, *Surf. Sci.*, 1993, **283**, 473.
27 M. Cieplak, E.D. Smith and M.O. Robbins, *Science*, 1994, **265**, 1209.
28 O.M. Braun, *The Frenkel-Kontorova Model: Concepts, Methods, and Applications*, Springer, 2004.
29 The small static friction at the sliding interface between two ideally hard disordered surfaces, e.g., metal on glass has also been discussed [19,30].
30 A. Erdemir and J.-M. Martin, *Superlubricity*, Elsevier Science Amsterdam, 2007.

This journal is © The Royal Society of Chemistry [year]

31 R. Zhang, Z. Ning, Y. Zhang, Q. Zheng, Q. Chen, H. Xie, Q. Zhang, W. Qian and F. Wei, *Nature Nanotech.*, 2013, **8**, 912.

32 A. Nigues, A. Siria, P. Vincent, P. Poncharal and L. Bocquet, *Nature Mater.*, 2014, **13**, 688.

33 M. Dienwiebel, G.S. Verhoeven, N. Pradeep, J.W. Frenken, J.A. Heimberg and H.W. Zandbergen, *Phys. Rev. Lett.*, 2004, **92**, 126101.

34 A. Filippov, M. Dienwiebel, J.W. Frenken, J.Klafter and M. Urbakh, *Phys. Rev. Lett.*, 2008, **100**, 046102.

35 M. M. van Wijk, M. Dienwiebel, J. W. M. Frenken and A. Fasolino, *Phys. Rev. B*, 2013, **88**, 235423.

36 A. Schirmeisen and U. D. Schwarz, *Chem. Phys. Chem.*, 2009, **10**, 2373.

37 T. Bohlein, J. Mikhael and C. Bechinger, *Nature Mater.*, 2012, **11**, 126.

38 A. Vanossi, N. Manini and E. Tosatti, *Proc. Natl. Acad. Sci. USA*, 2012, **109**, 16429.

39 A. Vanossi and E. Tosatti, *Nature Mater.*, 2012, **11**, 97.

40 P. Zeppenfeld, U. Becher, K. Kern and G. Comsa, *Phys. Rev. B*, 1992, **45**, 5179.

41 L. W. Bruch, R. D. Diehl and J. A. Venables, *Rev. Mod. Phys.*, 2007, **79**, 1381.

42 L. Bruschi, A. Carlin and G. Mistura, *Phys. Rev. Lett.*, 2002, **88**, 046105.

43 L. Bruschi, G. Fois, A. Pontarollo, G. Mistura, B. Torre, F. Buatier de Mongeot, C. Boragno, R. Buzio and U. Valbusa, *Phys. Rev. Lett.*, 2006, **96**, 216101.

44 L. Bruschi, M. Pierno, G. Fois, F. Ancilotto, G. Mistura, C. Boragno, F. Buatier de Mongeot and U. Valbusa, *Phys. Rev. B.*, 2010, **81**, 115419.

45 Ji-Yong Park et al., *Phys. Rev. B*, 1999, **60**, 16934.

46 R.L. Renner, J.E. Rutledge and P. Taborek, *Phys. Rev. B*, 2001, **63**, 233405.

47 G. Mistura, private communication.

48 K. Kern, P. Zeppenfeld, R. David and G. Comsa, *Phys. Rev. Lett.*, 1987, **59**, 79.

49 Note that QCM oscillations, of typical frequency $f_0 \sim 10\,\mathrm{MHz}$, are essentially static on the simulation timescales.

50 M. R. Sorensen, K. W. Jacobsen and P. Stoltze, *Phys. Rev. B*, 1996, **53**, 2101.